Gi-Chul Yang · Sio-Iong Ao
Len Gelman *Editors*

Transactions on Engineering Technologies

World Congress on Engineering 2014

Springer

Transactions on Engineering Technologies

Gi-Chul Yang • Sio-Iong Ao • Len Gelman
Editors

Transactions on Engineering Technologies

World Congress on Engineering 2014

Springer

Editors
Gi-Chul Yang
Multimedia Engineering
College of Engineering
Mokpo National University
Chonnam, Korea
Republic of (South Korea)

Len Gelman
Department of Applied
Mathematics & Computing
School of Engineering
Cranfield University
Cranfield, Bedfordshire, UK

Sio-Iong Ao
IAENG Secretariat
International Association of Engineers
Hong Kong, Hong Kong SAR

ISBN 978-94-017-9803-7 ISBN 978-94-017-9804-4 (eBook)
DOI 10.1007/978-94-017-9804-4

Library of Congress Control Number: 2015936284

Springer Dordrecht Heidelberg New York London
© Springer Science+Business Media Dordrecht 2015
This work is subject to copyright. All rights are reserved by the Publisher, whether the whole or part of the material is concerned, specifically the rights of translation, reprinting, reuse of illustrations, recitation, broadcasting, reproduction on microfilms or in any other physical way, and transmission or information storage and retrieval, electronic adaptation, computer software, or by similar or dissimilar methodology now known or hereafter developed.
The use of general descriptive names, registered names, trademarks, service marks, etc. in this publication does not imply, even in the absence of a specific statement, that such names are exempt from the relevant protective laws and regulations and therefore free for general use.
The publisher, the authors and the editors are safe to assume that the advice and information in this book are believed to be true and accurate at the date of publication. Neither the publisher nor the authors or the editors give a warranty, express or implied, with respect to the material contained herein or for any errors or omissions that may have been made.

Printed on acid-free paper

Springer Science+Business Media B.V. Dordrecht is part of Springer Science+Business Media (www.springer.com)

Preface

A large international conference on Advances in Engineering Technologies and Physical Science was held in London, U.K., 2–4 July, 2014, under the World Congress on Engineering 2014 (WCE 2014). The WCE 2014 is organized by the International Association of Engineers (IAENG); the Congress details are available at: http://www.iaeng.org/WCE2014. IAENG is a non-profit international association for engineers and computer scientists, which was founded originally in 1968. The World Congress on Engineering serves as good platforms for the engineering community to meet with each other and to exchange ideas. The conferences have also struck a balance between theoretical and application development. The conference committees have been formed with over 300 committee members who are mainly research center heads, faculty deans, department heads, professors, and research scientists from over 30 countries. The congress is truly global international event with a high level of participation from many countries. The response to the Congress has been excellent. There have been more than 900 manuscript submissions for the WCE 2014. All submitted papers have gone through the peer review process, and the overall acceptance rate is 51 %.

This volume contains 51 revised and extended research articles written by prominent researchers participating in the conference. Topics covered include mechanical engineering, bioengineering, internet engineering, wireless networks, signal and image engineering, manufacturing engineering, and industrial applications. The book offers the state of art of tremendous advances in engineering technologies and physical science and applications, and also serves as an excellent reference work for researchers and graduate students working on engineering technologies and physical science and applications.

Chonnam, Korea, Republic of (South Korea) — Gi-Chul Yang
Hong Kong, Hong Kong SAR — Sio-Iong Ao
Cranfield, Bedfordshire, UK — Len Gelman

Contents

1 Numerical Study of Conjugate Natural Convection from Discrete Heat Sources 1
Farouq A. Gdhaidh, Khalid Hussain, and Hong-Sheng Qi

2 Study of Soil-Structure Interaction Problems Using Mixed FEM-BEM Formulations 17
Dimas Betioli Ribeiro and João Batista de Paiva

3 A Study of the Reliability of Electronic Telecommunication Systems Working at Subsea Level 35
Sabuj Mallik and Franziska Kaiser

4 The Navier-Stokes Problem in Infinite Space 49
Kulyash Kaliyeva and Asset Kaliyev

5 Transient Problem for a Accreted Thermoelastic Block 67
Alexander L. Levitin and Sergei A. Lychev

6 Developing of a 1-D Combustion Model and Study of Engine Performance and Exhaust Emission Using Ethanol-Gasoline Blends 85
Simeon Penchev Iliev

7 An Approach to Modeling of Additive Manufacturing Technologies . 99
Alexander V. Manzhirov and Sergei A. Lychev

8 Analysis of the Cutting Forces in Manufacturing Stainless Steel Femoral Heads Using Finite Element Method 117
Nikolaos I. Galanis and Dimitrios E. Manolakos

9 Flowslide Investigations Test Rig Design 131
Giandomenico Di Massa, Luca Pagano, Stefano Pagano, Michele Russo, Riccardo Russo, and Maria Claudia Zingariello

10 Influence of Wire EDM on Fracture Toughness of TI6AL4V 147
Daniel M. Madyira and Esther T. Akinlabi

11 Accuracy of Available Methods to Evaluate Vierendeel Failure Load 163
Pattamad Panedpojaman and Worathep Sae-Long

12 Influence of Tibial Translation on Estimates of Patellar Tendon Force During Knee Flexion 177
Ahmed Imran

13 Numerical Simulation of the Aerodynamic Loads on Trees During Storms 187
Edward Chern Jinn Gan and Salim Mohamed Salim

14 Effecting Quench Agitation by Immersion Speed Variation of C30 Carbon Steel and Mechanical Properties Examination 201
Segun Mathew Adedayo, Adebayo Surajudeen Adekunle, and Tunji Ebenezer Oladimeji

15 Ventilation Flow Through a Room Fitted with a Windcatcher Using a LES CFD Technique 213
Amirreza Niktash and B. Phuoc Huynh

16 Visualising Dynamic Stall Around a Vertical Axis Wind Turbine Blade Through Particle Image Velocimetry 223
Okeoghene Eboibi, Jonathan Edwards, Robert Howell, and Louis Angelo Danao

17 Discrete and Continuous Growth of Deformable Cylinder 239
Sergei A. Lychev, Alexander V. Manzhirov, and Pavel S. Bychkov

18 Design and Characterization of a Model Pilot Multi-tube for the Transfer of Heating the Fire Tube Boilers in Academic Laboratories 255
Austin Ikechukwu Gbasouzor

19 Experimental and Computational Studies on Effects of Scale-Up of Riser on Heat Transfer Chatacterisitcs of Circulating Fluidized Bed 289
Ranjit S. Patil, Pinakeswar Mahanta, and Manmohan Pandey

20 Predicting the Influence of the Machining Parameters on the Tool Tip Temperature 305
S.A. Chowdhury, M.N. Islam, and B. Boswell

21 Production Planning for Make-to-Order Flow Shop System Under Hierarchical Workforce Environment 317
Sujan Piya and Nasr Al-Hinai

22 A Conceptual Framework for Analysing Supply Chain Performance of Oil Palm Refinery in Malaysia 331
Fitra Lestari, Kamariah Ismail, Abu Bakar Abdul Hamid, Eko Supriyanto, and Wahyudi Sutopo

23 Investigations on Abrasive Electrochemical Grinding Process (AECG) 341
Jerzy Kozak and Grzegorz Skrabalak

24 Pre-cooling Effects on the Resulting Grain Size in Friction Stir Processing of AZ31B 355
Ali H. Ammouri, Ghassan T. Kridli, George Y. Ayoub, and Ramsey F. Hamade

25 Survey on Simulation Methods in Multi-axis Machining 367
Khadidja Bouhadja and Mohamed Bey

26 An Approach to Modelate Human Error on Biodiesel Plants: Analysis of Active Failures and Latent Conditions 383
R.D. Calvo Olivares, S.S. Rivera, and J.E. Núñez Mc Leod

27 Exploring Pareto Frontiers in the Response Surface Methodology ... 399
Nuno Ricardo Costa and João Alves Lourenço

28 The Implications of Wet and Dry Turning on the Surface Quality of EN8 Steel 413
Zulfiqar Ahmad Khan, Matthew Grover, and Mian Hammad Nazir

29 Variable Selection Methods for Process Monitoring 425
Luan Jaupi

30 Grouping of Visible Terminals for Achieving High Throughput of Wireless Networks 437
Kengo Michishita and Yasushi Wakahara

31 Experimental Study on RSS Based Indoor Positioning Algorithms .. 451
Hélder David Malheiro da Silva, José Augusto Afonso, and Luís Alexandre Rocha

32 Study and Simulation of Protocols of WSN Using NS2 467
Ouafaa Ibrihich, Salah-ddine Krit, Jalal Laassiri, and Said El Hajji

33 Building Successfull Brand on the Internet 481
Tina Vukasović

34 An Active Integrated Zigbee RFID System with GPS Functionalities for Location Monitoring Utilizing Wireless Sensor Network and GSM Communication Platform 495
Farhana Ahmad Poad and Widad Ismail

35 Leveraging MMWAVE Technology for Mobile Broadband/Internet of Things 507
Oluwadamilola Oshin, Oluyinka Oni, Aderemi Atayero, and Babasanjo Oshin

36 Fast Power-Efficient Techniques for Collision Detection in Wireless Sensor Networks 515
Fawaz Alassery, Walid Ahmed, Mohsen Sarraf, and Victor Lawrence

37 Power Aware Virtual Path Routing Protocol for Cognitive Radio Ad Hoc Networks 531
Farhan Mahmud, Qurratulain Minhas, Hasan Mahmood, Zia Muhammad, and Hafiz Malik

38 Performance Evaluation of VoIP QoS Parameters Using WiFi-UMTS Networks 547
Mahdi Hassan Miraz, Muzafar Aziz Ganie, Maaruf Ali, Suhail Ahmed Molvi, and AbdelRahman Hamza Hussein

39 Extended Performance Studies of Wi-Fi IEEE 802.11 A, B, G Laboratory Wep Point-to-Multipoint and Point-to-Point Links.... 563
J.A.R. Pacheco de Carvalho, C.F. Ribeiro Pacheco, A.D. Reis, and H. Veiga

40 Deterministic Ethernet Using a Network Traffic Oscillator 573
Yuen Kwan Mo, Mark S. Leeson, and Roger J. Green

41 Cryptographic Adversary Model: Timing and Power Attacks 585
Mohd Anuar Mat Isa, Habibah Hashim, Amir Hamzah Abd Ghafar, Jamalul-lail Ab Manan, Syed Farid Syed Adnan, and Ramlan Mahmod

42 Using Elliptic Curve Encryption and Decryption for Securing Audio Messages 599
Artan Luma, Besnik Selimi, and Lirim Ameti

43 A Series of Secret Keys in a Key Distribution Protocol 615
Mohd Anuar Mat Isa, Habibah Hashim, Jamalul-lail Ab Manan, Syed Farid Syed Adnan, and Ramlan Mahmod

44 Forensics Issues in Cloud Usage 629
William R. Simpson

45 Undergraduate Student Retention Prediction Using Wavelet Decomposition 643
Ji-Wu Jia and Manohar Mareboyana

46 Construction of Radar SAR Images from Digital Terrain Model and Geometric Corrections 657
Philippe Durand, Luan Jaupi, and Dariush Ghorbanzadeh

47 Traffic Light Control Based on the Road Image Analysis 669
Obada M.A. Bani Issa, Venus W. Samawi, and Jehad Q. Alnihoud

48 On Cellular Automata Framework for Image Processing Hardware . 687
Abdul Raouf Khan and Md. Al-Amin Bhuiyan

49 Dynamic Simulation of the Temporomandibular Joint 697
Janith Muhandiram, Bin Wang, and Mahmoud Chizari

50 Using Information Gain to Compare the Effeciency of Machine Learning Techniques When Classifying Influenza Based on Viral Hosts 707
Nermin Shaltout, Ahmed Rafea, Ahmed Moustafa, and Mahmoud ElHefnawi

51 Process Optimization, Empirical Modeling and Characterization of Biodiesel from Cottonseed Oil 723
Umaru Musa, Aboje Audu Alechenu, Ibrahim Aris Mohammed, Aliyu Musa Aliyu, Muhammad Munir Sadiq, and Aminat Oladunni Olaibi

Erratum E1

Author Index 739

Subject Index 757

Chapter 1
Numerical Study of Conjugate Natural Convection from Discrete Heat Sources

Farouq A. Gdhaidh, Khalid Hussain, and Hong-Sheng Qi

Abstract The coupling between natural convection and conduction within rectangular enclosure was investigated numerically. Three separate heat sources were flush mounted on a vertical wall and an isoflux condition was applied at the back of heat sources. The governing equations were solved using control volume formulation. A modified Rayleigh number and a substrate/fluid thermal conductivity ratio were used in the range $10^4 - 10^7$ and $10 - 10^3$ respectively. The investigation was extended to examine high thermal conductivity ratio values. The results illustrated that, when Rayleigh number increased the dimensionless heat flux and local Nusselt number increased and the boundary layers along hot, cold and horizontal walls were reduced significantly. An opposite behaviour for the thermal spreading in the substrate and the dimensionless temperature, were decreased for higher Rayleigh number. Moreover, the thermal spreading in the substrate increased for higher substrate conductivity, which affected the temperature level. However the effect of the substrate is negligible when the thermal conductivity ratio higher than 1,500.

Keywords CFD study • Conjugate heat transfer • Control volume • Natural convection • Rayleigh number • Thermal conductivity

1 Introduction

Coupling between natural convection and conduction heat transfer is evident in many practical applications. In natural convection the fluid movement is created by the buoyancy force due to the temperature difference. Therefore no external force such as fans or coolers are needed which could be the main cause of noise and vibration. The conducting solid wall could also give additional heat transfer from the heat source to the fluid. The main drawback of natural convection is the rate of heat transfer is small compared to forced convection. Previous researches showed, this problem could be overcome by immersing the system in dielectric liquid [1].

F.A. Gdhaidh (✉) • K. Hussain • H.-S. Qi
Faculty of Engineering and Informatics, University of Bradford, Bradford BD7 1DP, UK
e-mail: F.A.Gdhaidh@bradford.ac.uk; K.Hussain1@bradford.ac.uk; H.Qi@bradford.ac.uk

© Springer Science+Business Media Dordrecht 2015

G.-C. Yang et al. (eds.), *Transactions on Engineering Technologies*,
DOI 10.1007/978-94-017-9804-4_1

Zinnes [2] investigated the conjugate effects in natural convection. He observed that, the coupling between conduction in a substrate and convection in a fluid is hugely affected by the substrate/fluid thermal conductivity ratio. Most of the published works in the field of natural convection from rectangular enclosures [3–5] whether these enclosures considered vertical or horizontal revealed that, the isothermal condition was applied to create temperature gradient. Several numerical investigations [6, 7] considered the conjugate natural convection from a heater mounted on a substrate immersed in liquid within an enclosure. It was concluded that most of the generated power was dissipated by the substrate for high value of substrate/fluid thermal conductivity ratio and the maximum temperature of the heater was decreased.

Heindel et al. [8] carried out a 3-D numerical and experimental study. Water and FC-77 were used within the enclosure and an isothermal cold wall at room temperature was assumed. They concluded that when the applied heat flux went up the convection coefficients and vertical velocity along heater faces increased. In addition, the flow inside the cavity became very complex when the Rayleigh number increased. Moreover, the 2-D numerical predictions exceeded those of 3-D model by 10–15 %. Further work by Heindel et al. [9] showed that the heat transfer was enhanced as much as 15 and 24 times for horizontal and vertical cavity orientations respectively by installing fins on the discrete heaters. The cold wall kept isothermally at 15 °C by using parallel plate fin arrays.

Numerical predictions of steady state natural convection in a square cavity was given by Banerjee et al. [10] to determine the sizes of heaters and the value of applied heat fluxes to ensure the operation within the specified thermal limit. Wroblewski and Joshi [11, 12] noticed that, at high substrate/fluid thermal conductivity ratio $R_s > 10$, the effects of the substrate conductivity especially on the maximum temperature were found to be very important due to the low thermal conductivity of the coolant liquid (FC-75). Experimental and numerical studies of conjugate heat transfer on a heated vertical wall were studied by Bilgen [13]. It was noticed that the Nusselt number depended on the Rayleigh number and wall thickness but it was a weak function of conductivity ratio. The thermal performance of the enclosure was improved with an increase in the Rayleigh number as reported in [14, 15]. Hyun and Kim [16] noticed that, in the case when the fluid confined between two plates, the temperature difference had to exceed a certain value between the plates before fluid motion could be detected.

Many efforts from previous studies using both numerical and experimental methods are focused on investigation of the effects of Rayleigh number R_a, substrate/fluid thermal conductivity ratio R_s and different fluids on the flow and temperature fields. It is shown that the maximum temperature is decreased with increasing R_s especially when $R_s > 10$. In the present study, numerical investigation was carried out, which shows that although the maximum temperature is reduced by increasing R_s, but there is a limit on R_s where the maximum temperature remains constant with increasing R_s over that limit.

2 Problem Description

A 2-D numerical investigation of the coupling between conduction and natural convection heat transfer from three discrete heat sources mounted on vertical wall of a cavity is presented. The opposite vertical wall and the horizontal walls are assumed to be at constant temperature (isothermal) and adiabatic respectively. Figure 1.1 shows a schematic of the two-dimensional rectangular cavity filled with different fluids of FC-77 (a dielectric fluorocarbon liquid) and air used in this investigation. The isoflux condition is applied at the back of each heat source whereas the back of the substrate was assumed to be adiabatic.

The height and length of the cavity where assumed as H and $(L_s + L_f)$ respectively. Aspect ratio of the cavity is fixed at $(A_z = H/L_f = 8)$. Table 1.1 illustrates the dimension of the parameters in mm.

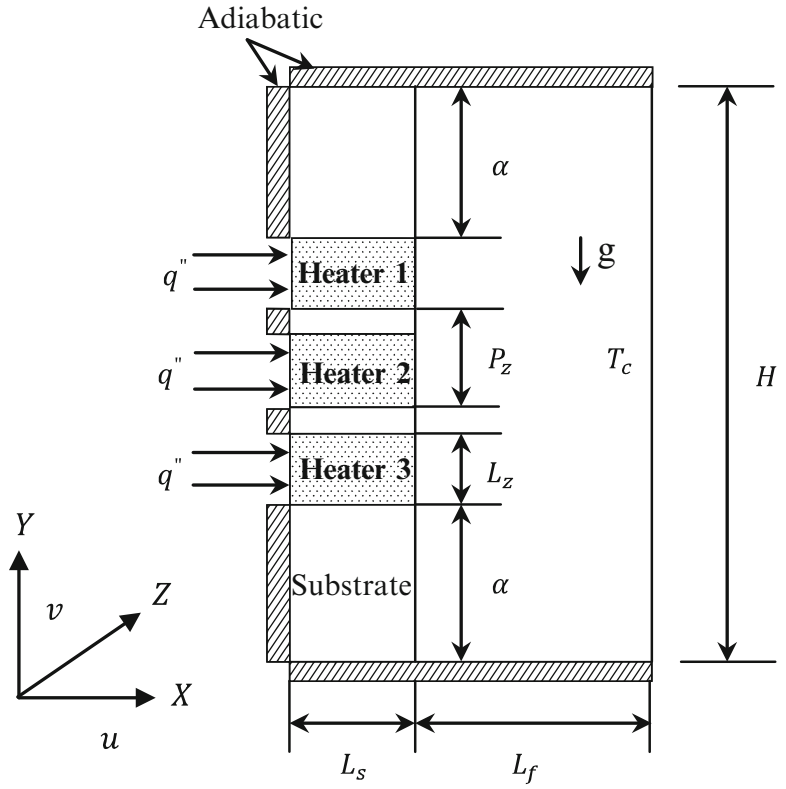

Fig. 1.1 A schematic diagram of the physical model

Table 1.1 Physical model parameters

H	L_z	P_z	L_f	L_s	α
96	12	16.8	12	6	25.2

3 Mathematical Model

The mathematical model is constrained by the following assumptions: 2-D steady state heat transfer, laminar natural convection flow without viscous dissipation, contact resistance between the heater/substrate interfaces and the radiation effects are neglected, the Boussinesq approximation is applied and the gravity acts in the vertical downward direction.

By using the above assumptions in the differential equations of continuity, momentum and energy, the governing equations are written in dimensionless form as:

- *In fluid region*:

  Continuity:

$$\frac{\partial U}{\partial X} + \frac{\partial U}{\partial Y} = 0 \tag{1.1}$$

  X-momentum:

$$U\ \frac{\partial U}{\partial X} + V\ \frac{\partial U}{\partial Y} = -\frac{\partial P}{\partial X} + P_r\ \left[\frac{\partial^2 U}{\partial X^2} + \frac{\partial^2 U}{\partial Y^2}\right] \tag{1.2}$$

  Y-momentum:

$$U\ \left[\frac{\partial V}{\partial X}\right] + V\ \left[\frac{\partial V}{\partial Y}\right] = -\left[\frac{\partial P}{\partial Y}\right] + P_r\ \left[\frac{\partial^2 V}{\partial X^2} + \frac{\partial^2 V}{\partial Y^2}\right] + R^*_{aL_z} P_r \theta \tag{1.3}$$

  Energy:

$$U\frac{\partial \theta}{\partial X} + V\frac{\partial \theta}{\partial Y} = \frac{\partial^2 \theta}{\partial X^2} + \frac{\partial^2 \theta}{\partial Y^2} \tag{1.4}$$

- *In solid region*:

  In this region there is only energy equation because the velocity components are zero, therefore the energy equation is written as:

$$K_1\frac{\partial^2 \theta}{\partial X^2} + K_2\frac{\partial^2 \theta}{\partial Y^2} = 0 \tag{1.5}$$

where K_1 and K_2 can be either the values of R_h or R_s depends on the position of the calculation whether in the heater or in the substrate region and:

$$R_s = \frac{k_s}{k_f},\ R_h = \frac{k_h}{k_f}$$

The above equations are obtained using the following dimensionless parameters:

$$X = \frac{x}{L_z},\ Y = \frac{y}{L_z},\ U = \frac{uL_z}{\alpha_f},\ V = \frac{vL_z}{\alpha_f} \tag{1.6}$$

$$P = \frac{p}{\rho\left(\alpha_f \Big/ L_z\right)^2},\ \theta = \frac{T - T_c}{\left(q'' L_z / k_f\right)} \tag{1.7}$$

$$R^*_{al_z} = \frac{g\beta q'' L_z^4}{k_f \alpha_f \nu}, \qquad P_r = \frac{\nu}{\alpha_f} \tag{1.8}$$

In order to complete the mathematical model, the following dimensionless boundary conditions are used:

- *At* $X = 0$:

$$U = V = 0,\ U = V = 0, \partial\theta/\partial X = \begin{cases} -1/R_h & at\ heater \\ 0 & at\ substrate \end{cases} \tag{1.9}$$

- *At* $X = \left(L_s + L_f\right)/L_z$:

$$U = V = 0,\ \theta = 0 \tag{1.10}$$

- *At* $Y = 0$:

$$U = V = 0,\ \frac{\partial\theta}{\partial Y} = 0 \tag{1.11}$$

- *At* $Y = H/L_z$:

$$U = V = 0,\ \frac{\partial\theta}{\partial Y} = 0 \tag{1.12}$$

The thermal conductivity for dissimilar materials is obtained by the harmonic mean formulation [17].

The local heat transfer coefficient at solid/fluid interface is defined as $h_s = q''/\left(T_{s(x)} - T_c\right)$ where $T_{s(x)}$ is the local temperature on the surface [10]. Therefore, the rate of convection heat transfer at any point in the solid/fluid interface wall is introduced by the dimensionless number (local Nusselt number $Nu(X)$) based on length of heat source, which is written as:

$$N_u(X) = -\frac{\Gamma}{\theta_w}\left(\frac{\partial\theta}{\partial X}\right)_w \tag{1.13}$$

4 Solution Procedure and Validation

In present study, the control volume technique was used to discretise the governing Eqs. (1.1, 1.2, 1.3, 1.4, and 1.5). The resulting algebraic equations were solved sequentially by "TDMA" (Tri-Diagonal Matrix Algorithm). The "SIMPLE" algorithm (semi-implicit method for pressure linked equations) was used to handle the coupling between pressure and velocity as described by Patankar [18]. To avoid the divergence in the iteration process, Under-relaxation techniques were used to slow down the change between iterations. It is noted that, although the solid and fluid regions have different equations, the numerical solutions within the computational domain for continuity, momentum and energy equations are obtained simultaneously in both regions.

The effect of the number of grid size ($Nx * Ny$) on the numerical analysis was carried out under the condition of the enclosure filled with FC-77 and $R^*_{al_z} = 10^4$. Three different uniform grid sizes were tested in both x and y directions. The results of dimensionless temperature at solid/fluid interface show that, the mesh size of $36 * 80$ gave an optimum computational time in comparison with other mesh sizes and also gave accurate results.

The code is validated against the benchmark results of Heindel et al. [18]. The validation results show that, dimensionless temperatures at solid/fluid interface have the same trends and the deviation between them decreases with increase of $R^*_{al_z}$. The biggest deviation was at the base of the enclosure with 11 % when $R^*_{al_z} = 10^4$ and the percentage is reduced to 6 % at the top of the enclosure.

5 Results and Discussion

The geometry used in this study is represented in Fig. 1.1. Firstly the numerical study examined the effects of modified Rayleigh number which is based on the

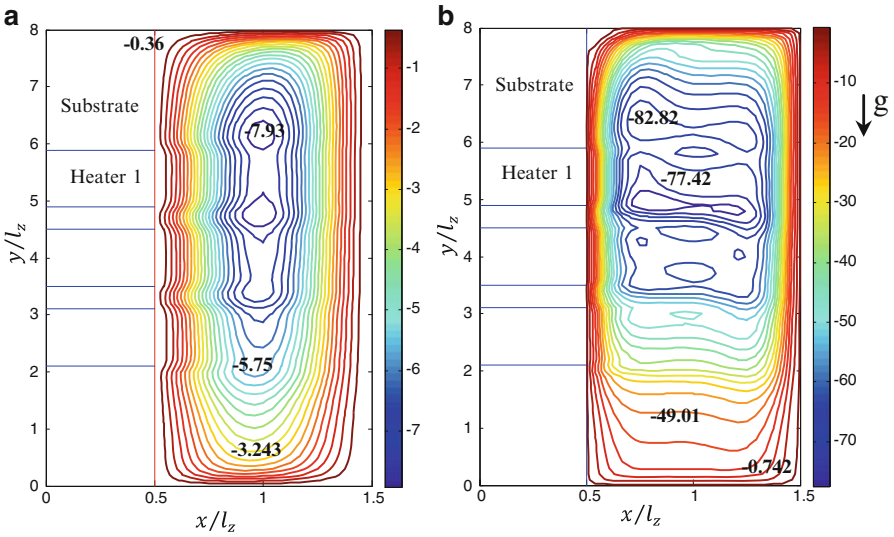

Fig. 1.2 Dimensionless streamlines ψ at (**a**) $R^*_{al_z} = 10^4$ and (**b**) $R^*_{al_z} = 10^7$ for FC-77 $P_r = 25$, $R_h = 2350$ and $R_s = 10$

applied isoflux condition in the range $R^*_{al_z} = 10^4 - 10^7$ for both fluids (FC-77 and air) and then the effect of thermal conductivity ratio R_s was examined in the range $10 - 1000$ for FC-77 only when the modified Rayleigh number fixed at 10^6.

5.1 Effects of Modified Rayleigh Number

Modified Rayleigh number was varied by changing the applied power to each heat source. The heaters' material used for the study was silicon with thermal conductivity ($k_h = 148\ W/mK$) producing constant heat flux and the heater/fluid thermal conductivity ratio is $R_h = 2350$ for FC-77 and $R_h = 5627$ for air. The fluid Prandtl number is assumed to be 25 corresponding to FC-77 and 0.7 for air, respectively. The flow field inside the enclosure is presented by dimensionless stream function as follow:

$$U = \partial\psi/\partial Y, \quad V = -\partial\psi/\partial X \tag{1.14}$$

Figures 1.2 and 1.3 illustrate the dimensionless streamlines for FC-77 and air respectively. Figure 1.2a represents the results for $R^*_{al_z} = 10^4$, where the flow is weak with $|\psi|_{max} = 7.93$, where ψ is an absolute value. There is a small core of nearly stagnant fluid located slightly above the centre of the enclosure, and the heaters regions are very clear.

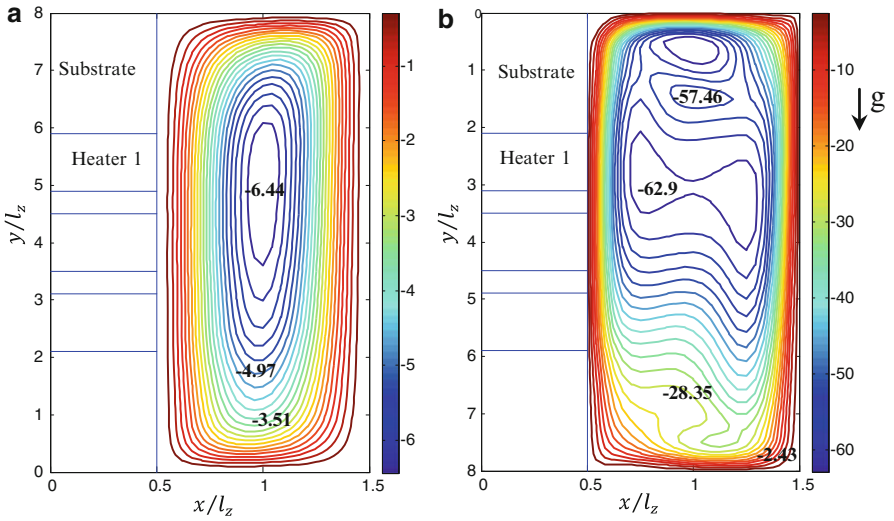

Fig. 1.3 Dimensionless streamlines ψ at (**a**) $R^*_{al_z} = 10^4$ and (**b**) $R^*_{al_z} = 10^7$ for air $P_r = 0.7$, $R_h = 5627$ and $R_s = 24$

Figure 1.3a shows that, the flow inside the enclosure for air is also weak with $|\psi|_{max} = 6.436$ but the flow is smooth. Additionally there is a thick thermal boundary layer along solid/fluid interface wall for both fluids.

It is noticed that, with increasing $R^*_{al_z}$ the boundary layers along hot, cold and horizontal walls become thinner. Also the flow developed in the central region of the cavity and becomes complex. Additionally as a result of the fluid circulation in clockwise direction, the cold fluid swept the hot fluid near the leading edge of each heater row and that is more noticeable for FC-77.

The dimensionless isotherms θ are shown in Figs. 1.4 and 1.5. For both fluids when $R^*_{al_z} = 10^4$, the contour lines of θ is nearly vertical in fluid region because the heat transfer is controlled by conduction. The lines for air are smoother than FC-77 where the effects of heater edges are clear.

With increasing $R^*_{al_z} = 10^7$ the central of fluid region is completely stratified and the thermal boundary layers of hot and cold walls are extremely thin. Because of the large thermal conductivity of heaters, each heater face is isothermal but the temperatures are different from one heater to another.

The dimensionless temperatures (θ) at solid/fluid interface for both fluids are studied and presented in Gdhaidh et al. [19]. The results indicate that, the dimensionless temperature decreases $R^*_{al_z}$ increase due to the increase in $(T - T_c)$ and hence not equal to the increase in q''.

Also the dimensionless local heat flux $\widehat{q}''$ and the local Nusselt number $Nu(X)$ are investigated. In general, both of $\widehat{q}''$ and $Nu(X)$ increase for higher Rayleigh number. For more details, see Gdhaidh et al. [19].

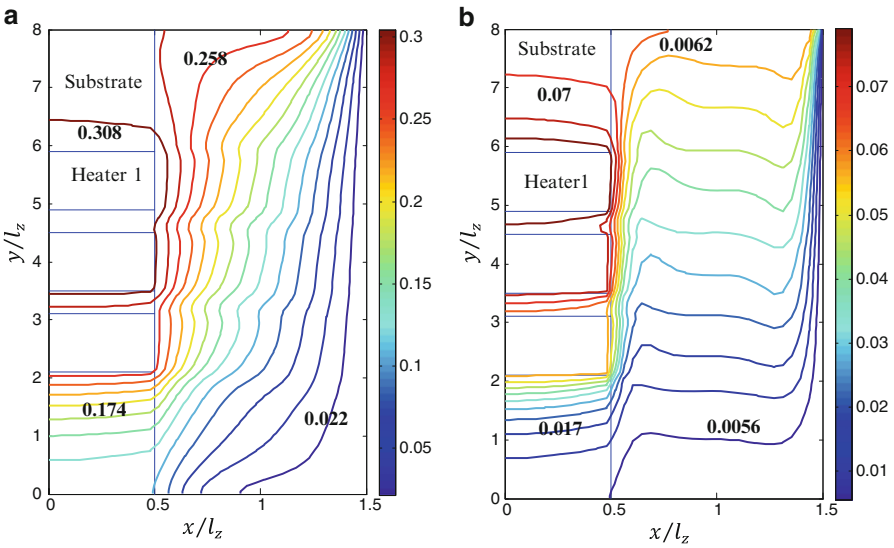

Fig. 1.4 Isotherms θ at (**a**) $R^*_{al_z} = 10^4$ and (**b**) $R^*_{al_z} = 10^7$ for FC-77 $P_r = 25$, $R_h = 2350$ and $R_s = 10$

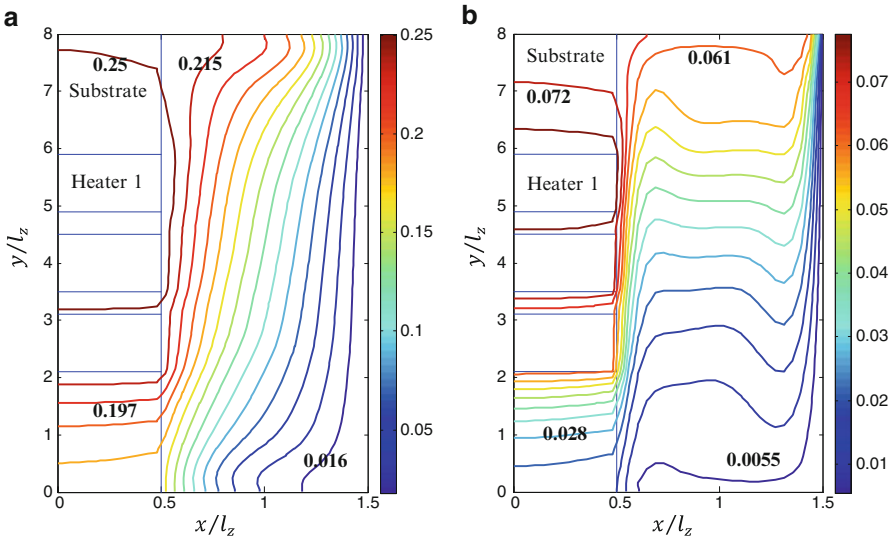

Fig. 1.5 Isotherms θ at: (**a**) $R^*_{al_z} = 10^4$ and (**b**) $R^*_{al_z} = 10^7$ for air $P_r = 0.7$, $R_h = 5627$ and $R_s = 24$

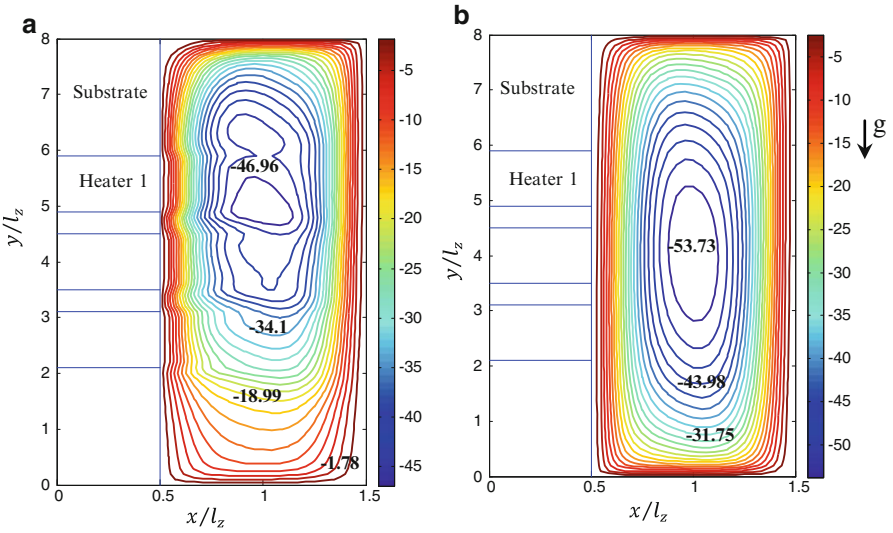

Fig. 1.6 Dimensionless streamline ψ at (**a**) $R_s = 10$ and (**b**) $R_s = 1000$ for FC-77 ($P_r = 25$, $R_h = 2350$ and $R^*_{al_z} = 10^6$)

5.2 *Effects of Substrate/Fluid Thermal Conductivity Ratio*

Further investigation was carried using FC-77 to study the effects of the substrate/fluid thermal conductivity ratio with a fixed modified Rayleigh number $R^*_{al_z} = 10^6$.

Figure 1.6 displays the dimensionless streamlines ψ for different values of R_s. It can be noticed that, the value of ψ increases from $|\psi|_{max} = 46.9$ when $R_s = 10$ to $|\psi|_{max} = 53.7$ when $R_s = 10^3$. As R_s increases, the flow pattern becomes smoother, and the stagnant core is located at the centre of the fluid region. The difference between the two streamlines in Fig. 1.6a, b is due to a higher thermal conductivity ratio for the case presented in Fig. 1.6b. Also the flow regions related to the discrete heaters become indistinguishable at high values of R_s, where the fluid below Heater 3 is preheated causing fluid movement. Additionally the flow is characterised by a clockwise circulation arising from the heaters due to the buoyancy effects.

Figure 1.7 shows the isotherms θ for different values of R_s. From the figure, the heaters' faces are isothermal but there are significant differences between the heaters' temperatures when $R_s = 10$. Those differences are due to the large thermal conductivity of the heaters and low thermal conductivity of the substrate. The heaters' temperature increases from Heater 3 to Heater 1 as a result of the increase in the local fluid temperature along the solid/fluid interface. For high value of $R_s = 10^3$, the maximum dimensionless temperature is decreased as more energy is dissipated by the substrate before being transported to the fluid. Moreover, the

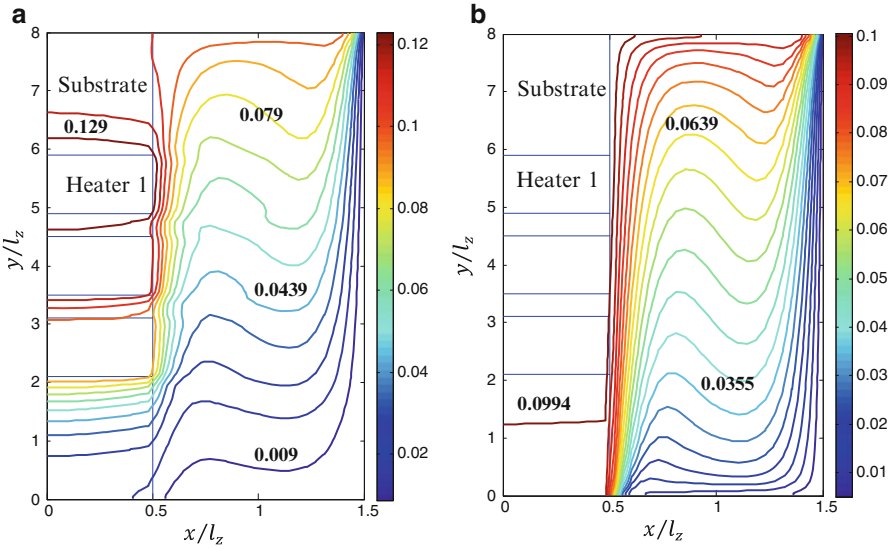

Fig. 1.7 Isotherms θ at (**a**) $R_s = 10$ and (**b**) $R_s = 1000$ for FC-77 ($\mathrm{P_r} = 25$, $R_h = 2350$ and $R^*_{al_z} = 10^6$)

heaters and substrate along the solid/fluid interface are approximately at the same temperature.

The dimensionless temperature distributions at the solid/fluid interface for different values of R_s are shown in Fig. 1.8. Increase in R_s gives another path to dissipate the heat from the heaters where more energy passes through the substrate. When the results from using two values of $R_s = 10$ and $R_s = 10^3$ are compared, there is a noticeable difference between them at the substrate region under Heater 3 where the dimensionless temperature of $R_s = 10^3$ is about 6 times higher than that of $R_s = 10$ at the base of the cavity. This difference decreases as y/l_z increase until $y/L_z = 3.5$, where the values of θ for $R_s = 10$ passes those of $R_s = 10^3$ and the maximum temperature when $R_s = 10^3$ is reduced by 23 %. Furthermore, the dimensionless temperature over the entire cavity height becomes nearly isothermal for large values of R_s.

In most applications, copper and aluminium are the preferred materials for the substrate. These two materials have a large thermal conductivity where the thermal conductivity ratios are 6,350 and 3,970 for copper and aluminium respectively. The results of θ along the solid/fluid interface are converged for both materials, also the heaters and substrate regions cannot be distinguished as shown in Fig. 1.8. Therefore, with very high values of R_s, the effect of thermal conductivity ratio on the dimensionless temperature is disappeared. As a result, the aluminium can be used instead of copper.

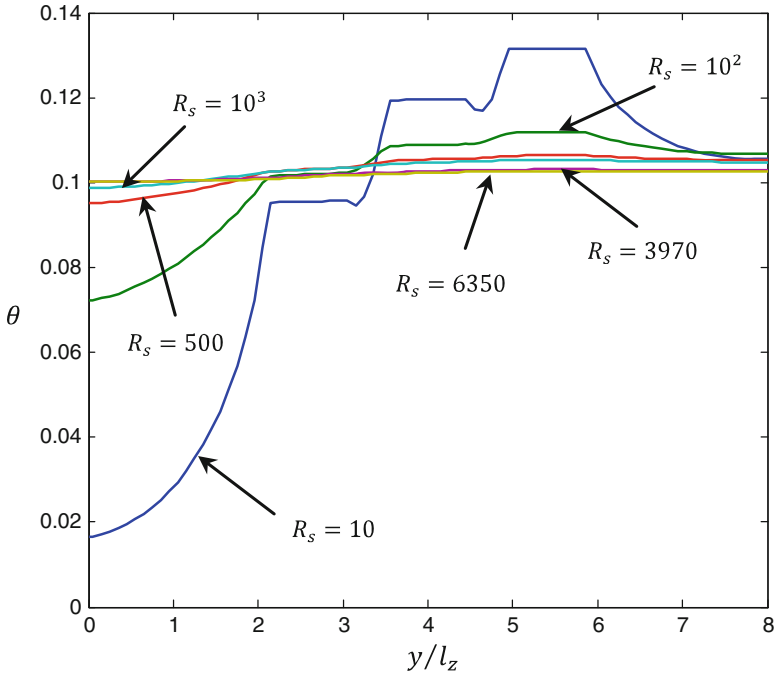

Fig. 1.8 Local dimensionless temperature distribution at the solid/fluid interface for FC-77 ($P_r = 25$, $R_h = 2350$ and $R^*_{al_z} = 10^6$)

5.3 *Temperature Results in Dimensional Form*

The previous results are presented in dimensionless form but it is important to know the value of the temperature in dimensional form. To present the temperature distribution at the solid/fluid interface in dimensional form (°C), as shown in Fig. 1.9 two values of modified Rayleigh number are selected, $R^*_{al_z} = 10^4$ and $R^*_{al_z} = 10^5$, for the given values of $R_s = 10$ and $R_s = 24$ for FC-77 and air respectively.

The value of q″ could be found from modified Rayleigh number equation $R^*_{al_z} = g\beta q'' L_z^4 / k_f \alpha_f \nu$ where the properties of FC-77 and air are known constant and the cold wall has a constant temperature of 20 °C. So the temperature in dimension form can be found from the following relation:

$$T = \frac{\theta q'' L_z}{K_f} + T_c \tag{1.15}$$

Table 1.2 shows the values of heat flux q'' for both working fluids at two selected modified Rayleigh number 10^4 and 10^5.

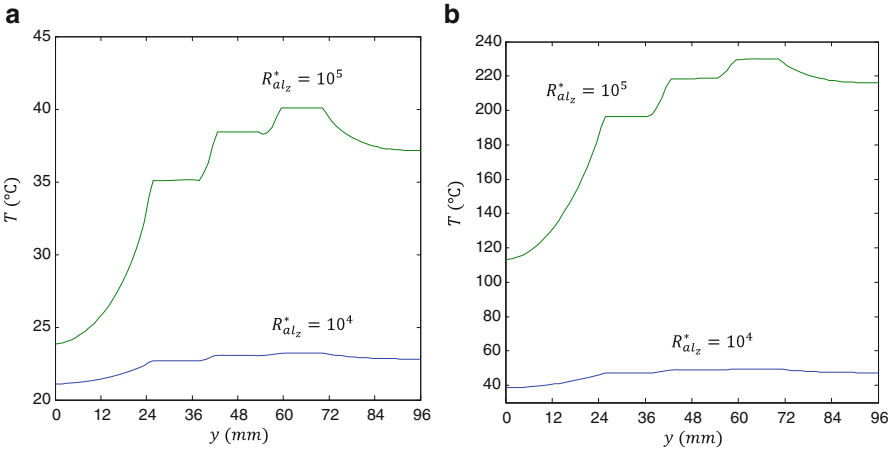

Fig. 1.9 Local dimension temperature distribution at the solid/fluid with different $R^*_{al_z}$: (**a**) for FC-77 and (**b**) for air

Table 1.2 The values of q″ for different modified Rayleigh number for both working fluids

$R^*_{al_z}$	$q''(W/m^2)$ for FC-77	$q''(W/m^2)$ for air
10^4	52.1	240
10^5	521	2400

6 Conclusions and Future Work

Steady state natural conjugate convection analysis for rectangular cavity with discrete heat sources flush mounted on one vertical wall has been conducted numerically. The control volume technique with the "SIMPLE" algorithm is used to simulate the problem. The results from this research show that:

1. At small values of modified Rayleigh number $R^*_{al_z} = 10^4$ the heat transfer is controlled by conduction. With increase $R^*_{al_z}$ the thermal boundary layers of the hot and cold walls become extremely thin and also the flow becomes more complex.
2. The dimensionless temperature θ at the solid/fluid interface for both working fluids (FC-77 and air) decreases as $R^*_{al_z}$ increases, due to the increment in the temperature differences is not equal to the increase in q''.
3. There is a strong effect of the substrate thermal conductivity on the temperature distribution as well as the maximum temperature. With increase R_s, more energy is dissipated by the substrate, which results in a decrease of the maximum temperature level.
4. For high values $R_s > 10^3$, the solid/fluid interface temperature becomes isothermal and the discrete heater locations become almost indistinguishable. Moreover when the $R_s > 1500$ the substrate has no effect on the maximum temperature.

In this study, an isothermal boundary conditions were is used. Such conditions are unrealistic for a normal desktop computer or other electronic devices. To keep one wall or more of the enclosure at a constant temperature, an adjustable water flow with pump and a heat exchanger is required. Moreover, when the ambient temperature is higher than the temperature of the walls, a refrigeration system is needed. Therefore, a large space is necessary and the levels of noise and vibration induced could be increased. In future study the above problem could be overcome by assuming the cold wall as a heat sink that is cooled by the air flow generated from the exhaust fan.

References

1. Bar-Cohen, A.: Physical design of electronic systems–methodology, technical trends, and future challenges. In: Advances in Thermal Modeling of Electronic Components and Systems, pp. 1–60. SME/IEEE Press, New York (1993)
2. Zinnes, A.E.: The coupling of conduction with laminar natural convection from a vertical fiat plate with arbitrary surface heating. J. Heat Transf. **92**, 528–535 (1970)
3. Hasnaoui, M., Bilgen, E., Vasseur, P.: Natural convection heat transfer in rectangular cavities heated from below. J. Thermophys. Heat Transf. **6**, 255–264 (1992)
4. Valencia, A., Frederick, R.L.: Heat transfer in square cavities with partially active vertical walls. Int. J. Heat Mass Transf. **32**, 1567–1574 (1989)
5. Selamet, E.E., Arpaci, V.S., Borgnakke, C.: Simulation of laminar buoyancy driven flows in an enclosure. Numer. Heat Transf. **22**, 401–420 (1992)
6. Sathe, S.B., Joshi, Y.: Natural convection arising from a heat generating substrate-mounted protrusion in a liquid-filled two-dimensional enclosure. Int. J. Heat Mass Transf. **34**, 2149–2163 (1991)
7. Du, Z.G., Bilgen, E.: Coupling of wall conduction with natural convection in a rectangular enclosure. Int. J. Heat Mass Transf. **35**, 1969–1975 (1992)
8. Heindel, T.J., Ramadhyani, S., Incropera, F.P.: Conjugate natural convection from an array of discrete heat sources: part 1 two- and three-dimensional model validation. Int. J. Heat Fluid Flow **16**, 501–510 (1995)
9. Heindel, T.J., Incropera, F.P., Ramadhyani, S.: Enhancement of natural convection heat transfer from an array of discrete heat sources. Int. J. Heat Mass Transf. **39**, 479–490 (1996)
10. Banerjee, S., Mukhopadhyay, A., Sen, S., Ganguly, R.: Natural convection in a bi-heater configuration of passive electronic cooling. Int. J. Therm. Sci. **47**, 1516–1527 (2008)
11. Wroblewski, D.E., Joshi, Y.: Computations of liquid immersion cooling for a protruding heat source in a cubical enclosure. Int. J. Heat Mass Transf. **36**, 1201–1218 (1993)
12. Wroblewski, D.E., Joshi, Y.: Liquid immersion cooling of a substrate-mounted protrusion in a three-dimensional enclosure: the effects of geometry and boundary conditions. J. Heat Transf. **116**, 112–119 (1994)
13. Bilgen, E.: Conjugate heat transfer by conduction and natural convection on a heated vertical wall. Appl. Therm. Eng. **29**, 334–339 (2009)
14. Aminossadati, S.M., Ghasemi, B.: Enhanced natural convection in an isosceles triangular enclosure filled with a nanofluid. Comput. Math. Appl. **61**, 1739–1753 (2011)
15. Sathe, S.B., Joshi, Y.: Natural convection liquid cooling of a substrate-mounted protrusion in a square enclosure: parametric study. Int. J. Heat Transf. **114**, 401–409 (1992)
16. Hyun, M.T., Kim, M.C.: Onset of buoyancy-driven convection in the horizontal fluid layer subjected to time-dependent heating from below. Int. Comm. Heat Mass Transf. **30**, 965–974 (2003)

17. Patankar, S.V.: Numerical Heat Transfer and Fluid Flow. McGraw-Hill, Washington (1980)
18. Heindel, T.J., Incropera, F.P., Ramadhyani, S.: Conjugate natural convection from an array of discrete heat sources: part 2 – a numerical parametric study. Int. J. Heat Fluid Flow **16**, 511–518 (1995)
19. Gdhaidh, F.A., Hussain, K., Qi, H.S.: Numerical investigation of conjugate natural convection heat transfer from discrete heat sources in rectangular enclosure. Lecture notes in engineering and computer science: proceedings of the world congress on engineering 2014, WCE 2014, pp. 1304–1309. London, 2–4 July (2014)

Chapter 2
Study of Soil-Structure Interaction Problems Using Mixed FEM-BEM Formulations

Dimas Betioli Ribeiro and João Batista de Paiva

Abstract The objective of this paper is to present formulations developed for soil-building interaction analysis, including foundations. The soil is modeled with the boundary element method (BEM) as a layered solid which may be finite for the vertical direction, but is always infinite for radial directions. Infinite boundary elements are employed for the far field simulation, allowing computational cost reduction without compromising the result accuracy. Beams, columns and piles are modeled with the finite element method (FEM) using one dimensional elements. Slabs and rafts are also modeled with the FEM, but with two dimensional elements. The analysis is static and all materials are considered homogeneous, isotropic, elastic and with linear behavior.

Keywords Boundary elements • Finite elements • Soil-structure interaction • Pile • Raft • Slab

1 Introduction

The construction of buildings involve complex soil-structure interaction effects that require previous studies to be correctly considered in the project. The basis of these studies has to be chosen among many options available and each one of them implies on advantages and disadvantages, as described below.

When possible, a good choice is to employ analytical methods. When correctly programmed they give trustful results in little processing time. In Ref. [2], for example, a solution is presented for an axially loaded pile with a rectangular cross section and immersed in a layered isotropic domain. The main disadvantage of

D.B. Ribeiro (✉)
Federal Institute of Education, Science and Technology of São Paulo, Rua Antonio Fogaça de Almeida, s/n, Jardim Elza Maria, Jacareí, SP, Brazil
e-mail: dimasbetioli@gmail.com

J.B. de Paiva
Department of Structural Engineering, School of Engineering of São Carlos, University of São Paulo, Av. Trabalhador Sãocarlense, 400, São Carlos, SP, Brazil
e-mail: paiva@sc.usp.br

© Springer Science+Business Media Dordrecht 2015

G.-C. Yang et al. (eds.), *Transactions on Engineering Technologies*,
DOI 10.1007/978-94-017-9804-4_2

these solutions is that they suit only specific situations, so many researches keep developing new ones to include new problems. Another reference that may be cited is [9].

If analytical solutions cannot be used, one alternative would be a numerical approach. The developments [6] of the numerical methods in the latter years and its versatility made them attractive to many researchers. The finite element method (FEM) is still popular [5, 16], however has some disadvantages when compared to other options such as the boundary element method (BEM). The FEM require the discretization of the domain, which has to be simulated as infinite in most soil-structure interaction problems. This implies on a high number of elements, leading to a large and sometimes impracticable processing time.

It becomes more viable solving these problems with the BEM, once only the boundary of the domains involved is discretized. This allows reducing the problem dimension, implying on less processing time. This advantage is explored in several works [1, 7, 12] and new developments are making the BEM even more attractive to future applications. One is simulating non-homogeneous domains using an alternative multi-domain BEM technique [13], another is using mapping functions to make boundary elements infinite [14].

The objective of this paper is to present a formulation for building-soil interaction analysis that uses recent developments accomplished by the authors in Refs. [13–15]. The proposed formulation is applied into two examples. In the first, a squared raft resting on an infinite layered domain is considered. Results are compared with other formulations available in the literature including an analytical approach and good agreement is observed. The objective of the second example is to show all functionalities of the proposed formulation, considering a complete building interacting with a layered soil. No comparison with other authors is presented, nevertheless the results obtained may be considered coherent. Finally, it is concluded that the presented formulation may be considered a practical and attractive alternative in the field of soil-structure interaction simulation.

2 Boundary Element Formulation

The equilibrium of a solid body can be represented by a boundary integral equation called the Somigliana Identity, which for homogeneous, isotropic and linear-elastic domains is

$$c_{ij}(y)\,u_j(y) + \int_{\Gamma} p^*_{ij}(x,y)\,u_j(x)\,d\Gamma(x) = \int_{\Gamma} u^*_{ij}(x,y)\,p_j(x)\,d\Gamma(x) \quad (2.1)$$

Equation 2.1 is written for a source point y at the boundary, where the displacement is $u_j(y)$. The constant c_{ij} depends on the Poisson ratio and the boundary geometry at y, as pointed out in Ref. [11]. The field point x goes through the whole

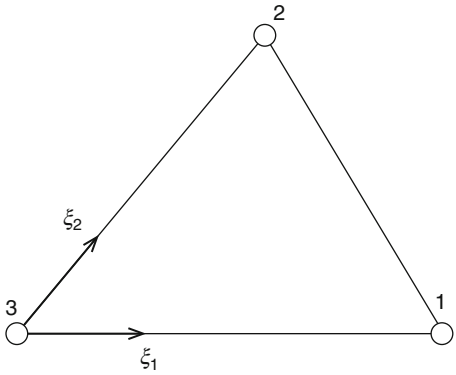

Fig. 2.1 Triangular boundary element

boundary Γ, where displacements are $u_j(x)$ and tractions are $p_j(x)$. The integral kernels $u^*_{ij}(x, y)$ and $p^*_{ij}(x, y)$ are Kelvin three-dimensional fundamental solutions for displacements and tractions, respectively. Kernel $u^*_{ij}(x, y)$ has order $1/r$ and kernel $p^*_{ij}(x, y)$ order $1/r^2$, where $r = |x - y|$, so the integrals have singularity problems when x approaches y. Therefore the stronger singular integral, over the traction kernel, has to be defined in terms of a Cauchy Principal Value (CPV).

To solve Eq. 2.1 numerically, the boundary is divided into regions within which displacements and tractions are approximated by known shape functions. Here these regions are of two types, finite boundary elements (BEs) and infinite boundary elements (IBEs). The BEs employed are triangular, as shown in Fig. 2.1 with the local system of coordinates, $\xi_1\xi_2$, and the local node numbering. The following approximations are used for this BE:

$$u_j = \sum_{k=1}^{3} N^k u_j^k, \quad p_j = \sum_{k=1}^{3} N^k p_j^k \tag{2.2}$$

Equation 2.2 relates the boundary values u_j and p_j to the nodal values of the BE. The BEs have 3 nodes and for each node there are three components of displacement u_j^k and traction p_j^k. The shape functions N^k used for these approximations are

$$N^1 = \xi_1, \quad N^2 = \xi_2, \quad N^3 = 1 - \xi_1 - \xi_2 \tag{2.3}$$

The same shape functions are used to approximate the boundary geometry and to interpolate displacements and tractions for the IBEs. The IBE geometry, on the other hand, is approximated by special mapping functions, as discussed in more detail in Sect. 3. By substituting Eq. 2.2 in 2.1, Eq. 2.4 is obtained:

$$c_{ij}u_j + \sum_{e=1}^{N_{BE}} \left\{ \sum_{k=1}^{3} \left[\Delta p_{ij}^{ek} u_j^k \right] \right\} + \sum_{e=1}^{N_{IBE}} \left\{ \sum_{k=1}^{Np} \left[\Delta^{\infty} p_{ij}^{ek} u_j^k \right] \right\}$$